




# Charged particles and quasiperiodic oscillations around magnetized Schwarzschild black holes

Mai Qi<sup>1,a</sup>, Javlon Rayimbaev<sup>2,3,4,b</sup> , Bobomurat Ahmedov<sup>4,5,6,c</sup>

<sup>1</sup> College of Creative Studies, University of California, Santa Barbara, CA 93106, USA

<sup>2</sup> School of Mathematics and Natural Sciences, New Uzbekistan University, Mustaqillik Ave. 54, 100007 Tashkent, Uzbekistan

<sup>3</sup> School of Engineering, Central Asian University, 111221 Tashkent, Uzbekistan

<sup>4</sup> Institute of Fundamental and Applied Research, National Research University “TIIAME”, Kori Niyoziy 39, 100000 Tashkent, Uzbekistan

<sup>5</sup> National University of Uzbekistan, 100174 Tashkent, Uzbekistan

<sup>6</sup> Ulugh Beg Astronomical Institute, Astronomy St. 33, Tashkent 100052, Uzbekistan

Received: 23 April 2023 / Accepted: 9 August 2023

© The Author(s) 2023

**Abstract** We study the motion of charged particles around Schwarzschild black holes immersed in external (i) asymptotically uniform, (ii) dipolar, and (iii) parabolic-like magnetic fields. The effect of the different magnetic-field configurations on the position of innermost stable circular orbits (ISCOs) for test-charged particles is analyzed. Furthermore, we investigated frequencies of radial and vertical oscillations of the charged particles along their stable circular orbits together with the Keplerian one. As an astrophysical application, we explore quasiperiodic oscillations (QPOs) observed in microquasars sourced by black hole candidates in the frame of the relativistic precession (RP) model. In order to obtain constraints on the values of the magnetic parameter and black hole mass for the microquasars GRO J1655-40 and GRS 1915-105, we use the method so-called  $\chi^2$  in the Bayesian approach. Also, we get constraints on the magnetic field around the black hole in the microquasars by treating electrons and protons as oscillating test-charged particles in the accretion disc. Our performed analyses show that the masses of black hole candidates in the above-mentioned objects and magnetic parameters are different for the uniform and dipolar magnetic field configurations. However, no constraints on the magnetic field and black hole masses are obtained in the case of a parabolic magnetic field configuration. The obtained results on the black hole masses are compared with the measurements in independent astrophysical observations of these black hole masses.

## 1 Introduction

In classical general relativity, black holes do not radiate in the electromagnetic spectrum, so it is not possible to directly obtain information about an isolated black hole. However, black holes' gravity in binary systems plays an important role in deriving all the radiation processes in the surrounding accretion disk. QPOs are one of the astrophysical phenomena in the electromagnetic spectrum found by using Fourier analyses of the noisy continuous X-ray data from the accretion disk in (micro)quasars. QPOs are called high-frequency (HF) when the peak frequencies are about 0.1–1 kHz and low-frequency (LF) when the frequencies are less than about 0.1 kHz peak. At present, a number of QPOs have been detected from the accretion disk surrounding not only black holes but also neutron stars and white dwarfs as well as their binary systems including companion stars [1–3]. Mostly, high-frequency Hz QPOs are observed in low-mass X-ray binaries (LMXBs) spectrum with different behaviors, suggesting that their origin mechanisms may differ. It has been proposed that QPOs from neutron star binary systems are strongly connected with the surface magnetic field of the star and its rotation period [4]. The mechanism of the electromagnetic emission from the accretion disk around the central black hole may be connected with particle oscillations along stable circular orbits. In fact, charged particles radiate with the frequency the same as their oscillation frequency. So, the dynamics of the charged test particles around black holes may explain the existence of QPOs based on their (quasi-)harmonic oscillations in radial and angular directions.

Despite lots of QPOs having been observed in such binary systems with high-accuracy measurements of the frequen-

<sup>a</sup> e-mail: [maiqi@ucsb.edu](mailto:maiqi@ucsb.edu)

<sup>b</sup> e-mail: [javlon@astrin.uz](mailto:javlon@astrin.uz) (corresponding author)

<sup>c</sup> e-mail: [ahmedov@astrin.uz](mailto:ahmedov@astrin.uz)

cies, no exact and unique physical mechanisms for QPOs have been found. The problem is still under active discussion in testing gravity theories and measurements of the inner edge of the accretion disc, which may help to get valuable information about ISCOs radii [5–7]. In our previous papers [8–11], we have shown that orbits of twin-peak QPOs with a frequency ratio close to 1 are located near ISCO with the distance in the order of error in observations. In this sense, the QPOs studies become a powerful tool to estimate the ISCO radius being the innermost regions of accretion disks as well as the central black hole mass, and more about gravity properties.

Microquasars are binary systems consisting of black holes & neutron stars and companion main sequence stars which can be observed as X-ray binary systems. Such systems containing gravitational compact objects may be helpful in testing gravity in a strong gravity regime. For the first time, QPOs have been discovered in analyses of the power spectra of X-ray flux from a low mass X-ray binary (LMXB) system [12]. The discovery of QPOs is also become a good study in testing the gravitational properties of the central object in microquasars [13]. Recent astrophysical measurements have provided precise information about the frequencies of twin-peaked QPOs that were observed with a ratio of 3 : 2 [13–15]. Several independent models explain the physical mechanisms in processes in QPOs by disk-seismic, hot-spot, warped disk, and resonance models, etc. [5, 7, 16–20].

Physical processes including electromagnetic radiation of charged particles in the accretion discs around black holes in both thin [21, 22] and thick accretion disc [23–30] models are formed by a non-linear interplay of various processes, such as gravity, viscosity, scattering, etc. and can be described by the magnetohydrodynamics (MHD) equations [31–44].

In this work, we plan to investigate charged particles' oscillations in the spacetime of the Schwarzschild black hole in the presence of external uniform, dipolar, and parabolic magnetic fields together with the applications to QPOs, and to obtain constraints on magnetic field strength and mass of the central black hole using the observed QPOs data.

The paper is organized as follows. Section 2 is devoted to studying uniform, dipolar, and parabolic magnetic fields around the Schwarzschild black hole. In Sect. 3 we calculate frequencies of the charged particle's radial and vertical oscillations at stable circular orbits around the Schwarzschild black hole in the presence of an external magnetic field with different configurations. The effects of the external magnetic field on upper and lower frequencies of twin peak QPOs are studied in Sect. 4. In Sect. 5 we have obtained constraints on the black hole mass at the center of the microquasars GRO J1655-40 and GRS 1915+105 using observed QPO frequencies. Finally, in Sect. 6 we summarize the main results obtained.

The spacetime is used with the signature  $(-, +, +, +)$ . The quantities are in the geometrized unit's system as  $G = c = 1$ . For astrophysical applications in converting the unit of frequency from  $cm^{-1}$  to Hz, we use the values of speed of light in a vacuum and gravitational constant as they are given in the Gaussian unit system. Furthermore, Latin indices take integer values from 1 to 3, while Greek ones take integer values from 0 to 3.

## 2 Charged test particles motion around a black hole in the presence of magnetic fields

In this section, we derive the equation of motion around the Schwarzschild black hole immersed in the above-mentioned external magnetic field configurations. The spacetime geometry around Schwarzschild black holes is written through spherical coordinates,  $(x^\alpha = \{t, r, \theta, \phi\})$  in the form,

$$ds^2 = -f(r)dt^2 + \frac{1}{f(r)}dr^2 + r^2d\Omega^2, \quad (1)$$

where the radial function  $f(r) = 1 - 2M/r$  and  $d\Omega^2 = d\theta^2 + \sin^2\theta d\phi^2$ .

### 2.1 External magnetic field configurations

Now, we assume that the Schwarzschild black hole is immersed in external magnetic fields with asymptotically uniform ( $u$ ), dipolar ( $d$ ), and parabolic ( $p$ ) configurations, and the electromagnetic four potentials for the fields can be expressed as follows [45–47]:

$$A_\phi = \frac{B_0}{2}\mathcal{H}_i(r)\mathcal{T}_i(\theta), \quad (2)$$

where  $i$  stands for  $u, d, p$  and

$$\mathcal{H}_u(r) = r^2, \quad \mathcal{T}_U(\theta) = \mathcal{T}_D(\theta) = \sin^2\theta, \quad (3)$$

$$\mathcal{H}_d(r) = r^2 \left[ \ln f(r) + \frac{2M}{r} \left( 1 + \frac{M}{r} \right) \right], \quad (4)$$

$$\mathcal{H}_p(r) = r^k, \quad \mathcal{T}_P(\theta) = 1 - |\cos\theta|, \quad (5)$$

where  $B_0$  is the asymptotic value of the external magnetic field,  $k$  is the declination of the field lines, and  $k = 3/4$  is the corresponding case of the parabolic shape of the external magnetic field [47].

One may immediately find the nonzero components of the electromagnetic field tensor using the definition  $F_{\mu\nu} = A_{\nu,\mu} - A_{\mu,\nu}$  for each configuration of the external magnetic field in the following form.

$$F_{r\phi} = \frac{1}{2}B_0\mathcal{H}'_i(r)\mathcal{T}_i(\theta), \quad (6)$$

$$F_{\theta\phi} = \frac{1}{2}B_0\mathcal{H}_i(r)\mathcal{T}'_i(\theta), \quad (7)$$

where ' denotes partial derivative over  $\mathcal{H}_i$  and  $\mathcal{T}_i$  is with respect to the coordinates  $r$  and  $\theta$ , respectively.

The components of the magnetic field around the black hole measured by a zero angular momentum observer (ZAMO) can be calculated as,

$$B^i = \frac{1}{2} \eta^{i\beta\sigma\mu} F_{\beta\sigma} w_{\mu}, \tag{8}$$

where  $i = (r, \theta, \phi)$ ,  $w_{\mu}$  is the four-velocity of the ZAMO with  $w^{\mu} = 1/\sqrt{f(r)}(1, 0, 0, 0)$ ,  $\eta_{\alpha\beta\sigma\gamma}$  is the pseudo-tensorial form of the Levi-Civita symbol  $\epsilon_{\alpha\beta\sigma\gamma}$  with the relations

$$\eta_{\alpha\beta\sigma\gamma} = \sqrt{-g} \epsilon_{\alpha\beta\sigma\gamma}, \quad \eta^{\alpha\beta\sigma\gamma} = -\frac{1}{\sqrt{-g}} \epsilon^{\alpha\beta\sigma\gamma}, \tag{9}$$

and  $g = \det|g_{\mu\nu}| = -r^4 \sin^2 \theta$  for spacetime metric (1)  $\epsilon_{0123} = 1$  with even permutations and  $-1$  for odd ones, and it is zero for other combinations. One can obtain expressions for the non-zero orthonormal components of the magnetic field using the tetrads carried by the ZAMO [48],

$$B^{\hat{r}} = B_0 \frac{\mathcal{H}_i(r) \mathcal{T}'_i(\theta)}{2r^2 \sin \theta}, \tag{10}$$

$$B^{\hat{\theta}} = B_0 \frac{\mathcal{H}'_i(r) \mathcal{T}_i(\theta)}{2r \sin \theta} \sqrt{f(r)}. \tag{11}$$

### 2.2 Equations of motion of charged particles in magnetized black hole environment

Here, we investigate the dynamics of charged particles in circular orbits around the magnetized Schwarzschild black hole using the Hamilton-Jacobi equation

$$g^{\mu\nu} \left( \frac{\partial \mathcal{S}}{\partial x^{\mu}} - q A_{\mu} \right) \left( \frac{\partial \mathcal{S}}{\partial x^{\nu}} - q A_{\nu} \right) = -m^2. \tag{12}$$

The action for charged particles at a constant plane (where  $\theta = const$  and  $\dot{\theta} = 0$ ) can be described by the following separable form,

$$\mathcal{S} = -Et + l\phi + \mathcal{S}_r + \mathcal{S}_{\theta}, \tag{13}$$

which allows for separating the variables in the Hamilton-Jacobi equation.

One may find the conserved quantities using the time independence of the metric tensor (1) and the external magnetic field in the following separable form:

$$\dot{t} = \frac{\mathcal{E}}{f(r)}, \quad \dot{\phi} = \frac{l}{g\phi\phi} - \omega_B, \tag{14}$$

where  $\omega_B = qB_0/(2mc)$  is the magnetic coupling parameter which corresponds to the interaction of the magnetic field and orbiting charged particle.

The equation for the radial motion of charged test particles can be found as

$$\dot{r}^2 = \mathcal{E}^2 - V_{\text{eff}}(r), \tag{15}$$

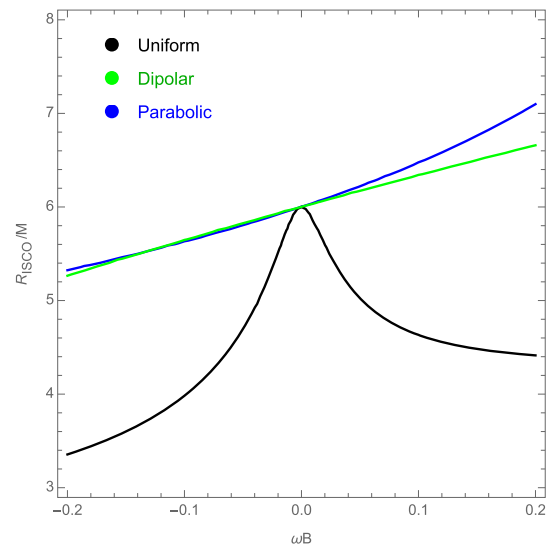


**Fig. 1** ISCO radius against  $\omega_B$  for uniform, dipolar, and parabolic magnetic fields

where  $\mathcal{E} = E/m$  is the specific energy of the particles and the effective potential for the radial motion of the charged particles has the following form:

$$V_{\text{eff}}(r) = f(r) \left\{ 1 + \frac{1}{g\phi\phi} [\mathcal{L} + \omega_B \mathcal{H}_i(r) \mathcal{T}_i(\theta)]^2 \right\}, \tag{16}$$

where  $\mathcal{L} = l/m$  is specific angular momentum of the particle.

### 2.3 Stable circular orbits

The stable circular orbits occur at the radius where the minimum of the effective potential takes place. The innermost stable circular orbits (ISCOs) which satisfy the conditions  $\partial_{rr} V_{\text{eff}} = 0$  and  $\partial_r \mathcal{L}_c = 0$  that gives the same results.

Figure 1 demonstrates the effect of the magnetic field on the ISCO radius around the Schwarzschild black hole. For all three cases,  $\omega_B = 0$  corresponds to  $R_{\text{ISCO}} = 6M$ , recovering the standard Schwarzschild result in the vacuum case. These graphs can be reflected across the  $\omega_B = 0$  line by the transformation  $\mathcal{L} \rightarrow -\mathcal{L}$ , which does not change the physics for a Schwarzschild black hole. It is seen that the effect of magnetic interaction causes decreasing the ISCO radius in the case of the uniform magnetic field. However, in the dipolar and parabolic magnetic field configuration cases, the positive values of  $\omega_B$  reduce the increase of ISCO radius.

## 3 Epicyclic frequencies for charged particles around magnetized Schwarzschild black hole

In this section, we study oscillations of charged particles around a Schwarzschild black immersed in the above-mentioned magnetic-field configurations. In fact, the periodi-

cal motion of the charged particles along stable circular orbits around black holes occurs at the orbits where  $r \geq r_{isco}$  and effective potential take minimum. The unperturbed circular motion is a non-geodesic motion obeying the equation,

$$\frac{du^\alpha}{d\tau} + \Gamma_{\mu\nu}^\alpha u^\mu u^\nu = \frac{q}{m} F_{\beta}^\alpha u^\beta, \tag{17}$$

where  $u^\mu$  is the four-velocity of the particle.  $\Gamma_{\mu\nu}^\alpha$  are Christoffel symbols related to the metric (1).

Now, we assume the charged particle is displaced from its circular position  $X^\mu$  by a very small  $\eta^\mu$  taking the actual position  $X^\mu = x^\mu + \eta^\mu$  and correspondingly, its four-velocity is  $U^\mu = u^\mu + \dot{\eta}^\mu$ .

Consequently, the modified non-geodesic equation takes the form

$$\frac{dU^\alpha}{d\tau} + \Gamma_{\mu\nu}^\alpha (X^\mu) U^\mu U^\nu = \frac{q}{m} F_{\beta}^\alpha u^\beta. \tag{18}$$

One may immediately get the equation of the oscillations of the particles using the above modified nongeodesic equation as

$$\begin{aligned} \ddot{\eta}^\mu + 2\Gamma_{\alpha\beta}^\mu u^\alpha \dot{\eta}^\beta + \partial_\nu \Gamma_{\alpha\beta}^\mu u^\alpha u^\beta \eta^\nu \\ = e (F_{\nu}^\mu \dot{\eta}^\nu + \partial_\lambda F_{\nu}^\mu u^\nu \eta^\lambda). \end{aligned} \tag{19}$$

Here, we are interested to study the oscillations in the radial and vertical directions and the corresponding harmonic oscillator equation which can be described as follows

$$\ddot{\eta}^i + \omega_i^2 \eta^i = 0, \quad \text{where } i = (r, \theta). \tag{20}$$

The  $\theta$  component,

$$\ddot{\eta}^\theta + \omega_\theta^2 \eta^\theta = 0, \tag{21}$$

$$\omega_\theta^2 = \partial_\theta \left( \Gamma_{ij}^\theta u^i u^j + e g^{\theta\theta} F_{i\theta} u^i \right), \quad (i, j = t, \theta). \tag{22}$$

After simple algebraic calculations, we have the frequency of vertical oscillations in the following form:

$$\begin{aligned} \omega_\theta^2 = \partial_\theta \Gamma_{tt}^\theta (u^t)^2 + 2\partial_\theta \Gamma_{t\phi}^\theta u^t u^\phi + \partial_\theta \Gamma_{\phi\phi}^\theta (u^\phi)^2 \\ + e \left[ \partial_\theta (g^{\theta\theta} F_{t\theta}) u^t + \partial_\theta (g^{\theta\theta} F_{\phi\theta}) u^\phi \right]. \end{aligned} \tag{23}$$

Similarly, one can calculate the oscillation frequencies in the radial directions,

$$\begin{aligned} \ddot{\eta}^r + \partial_r \left( \Gamma_{ij}^r u^i u^j + e g^{rr} F_{ir} u^i \right) \eta^r \\ + \left( 2\Gamma_{ji}^r u^i + e g^{rr} F_{jr} \right) \dot{\eta}^j = 0, \quad (i, j = t, \theta), \end{aligned} \tag{24}$$

where

$$\begin{aligned} \omega_r^2 = \partial_r \left( \Gamma_{ij}^r u^i u^j + e g^{rr} F_{ir} u^i \right) \\ + 2e \left( g^{ik} \Gamma_{kj}^r - g^{rr} \Gamma_{rj}^i \right) F_{ir} u^j + e^2 g^{rr} g^{ij} F_{ir} F_{jr} \\ - 4\Gamma_{ik}^r \Gamma_{rj}^k u^i u^j \quad (i, j, k = t, \phi). \end{aligned} \tag{25}$$

Thus, the Keplerian frequency ( $\omega_K = d\phi/dt$ ), can be calculated using the equations of motion,

$$\begin{aligned} \omega_k^2 = \left[ 1 + 4g_{\phi\phi} \left( \frac{qA_{\phi,r}}{mg_{\phi\phi,r}} \right)^2 \right]^{-1} \left\{ \omega_0^2 - 2g_{tt} \left( \frac{qA_{\phi,r}}{mg_{\phi\phi,r}} \right)^2 \right. \\ \left. \pm 2\omega_0^2 \frac{qA_{\phi,r}}{mg_{\phi\phi,r}} \sqrt{g_{\phi\phi} - \frac{g_{tt}}{\omega_0^2} + \left( \frac{g_{tt}}{\omega_0^2 g_{\phi\phi,r}} \right)^2} \right\}, \end{aligned} \tag{26}$$

and it is easy to see that for neutral particles case and/or in the absence of external magnetic field  $q = 0$ ,  $A_\phi = 0 \rightarrow qA_\phi = 0$ , the above equation turns simply to  $\omega_0^2 = -g_{tt,r}/g_{\phi\phi,r}$  that refers to the Keplerian frequency for the neutral particle orbiting the spherical symmetric black hole as  $\omega_k^2 = \omega_0^2 = M/r^3$ .

From Eqs. (25), (23) and (26) one can define epicyclic frequencies  $\omega_r$  and  $\omega_\theta$  as follows:

$$\begin{aligned} \omega_r^2 = \frac{g_{tt,r}^2}{g_{tt}g_{rr}} - \frac{g_{tt,rr}}{g_{rr}} + \frac{\omega_k^2}{g_{rr}} \left( \frac{g_{\phi\phi,r}^2}{g_{\phi\phi}} - \frac{g_{\phi\phi,rr}}{2} \right) \\ - \frac{q}{m} \frac{\omega_k}{g_{rr}} \left( A_{\phi,rr} - 2A_{\phi,r} \frac{g_{\phi\phi,r}}{g_{\phi\phi}} \right) \left( -g_{tt} - \omega_k^2 g_{\phi\phi} \right)^{1/2} \\ - \left( \frac{q}{m} \right)^2 \frac{A_{\phi,r}^2}{g_{rr}} \left( \omega_k^2 + \frac{g_{tt}}{g_{\phi\phi}} \right), \end{aligned} \tag{27}$$

$$\begin{aligned} \omega_\theta^2 = \frac{g_{tt,\theta}^2}{g_{tt}g_{\theta\theta}} - \frac{g_{tt,\theta\theta}}{g_{\theta\theta}} + \frac{\omega_k^2}{g_{\theta\theta}} \left( \frac{g_{\phi\phi,\theta}^2}{g_{\phi\phi}} - \frac{g_{\phi\phi,\theta\theta}}{2} \right) \\ - \frac{q}{m} \frac{\omega_k}{g_{\theta\theta}} \left( A_{\phi,\theta\theta} - 2A_{\phi,\theta} \frac{g_{\phi\phi,\theta}}{g_{\phi\phi}} \right) \left( -g_{tt} - \omega_k^2 g_{\phi\phi} \right)^{1/2} \\ - \left( \frac{q}{m} \right)^2 \frac{A_{\phi,\theta}^2}{g_{\theta\theta}} \left( \omega_k^2 + \frac{g_{tt}}{g_{\phi\phi}} \right). \end{aligned} \tag{28}$$

One can see that the expressions of the fundamental frequencies  $\omega_{k,r,\theta}$  have complicated forms. Therefore, we will present graphical analyses converting their units to Hz using the following expression:

$$\nu_{k,r,\theta} = \frac{1}{2\pi} \frac{c^3}{GM} \omega_{k,r,\theta}, \tag{29}$$

where  $G$  and  $c$  are the gravitational field constant and speed of light in vacuum. The above frequency can be measured by distant observers located at infinity and can be directly used to analyse the observed data.

Figure 2 presents the effect of different magnetic field configurations on the Keplerian ( $\nu_k = \nu_\phi$ ) and radial oscillation frequencies of a charged particle for the case of  $M = 5M_\odot$ . For the Keplerian frequency, the particle in a uniform field configuration is much more sensitive to the value of  $\omega_B$  than in dipolar and parabolic fields. Furthermore, as  $r/M \rightarrow \infty$ ,  $\nu_k$  approaches the classical cyclotron frequency instead of decreasing to 0 in the uniform field with non-zero  $\omega_B$ . This is expected since as the distance from the black hole increases,

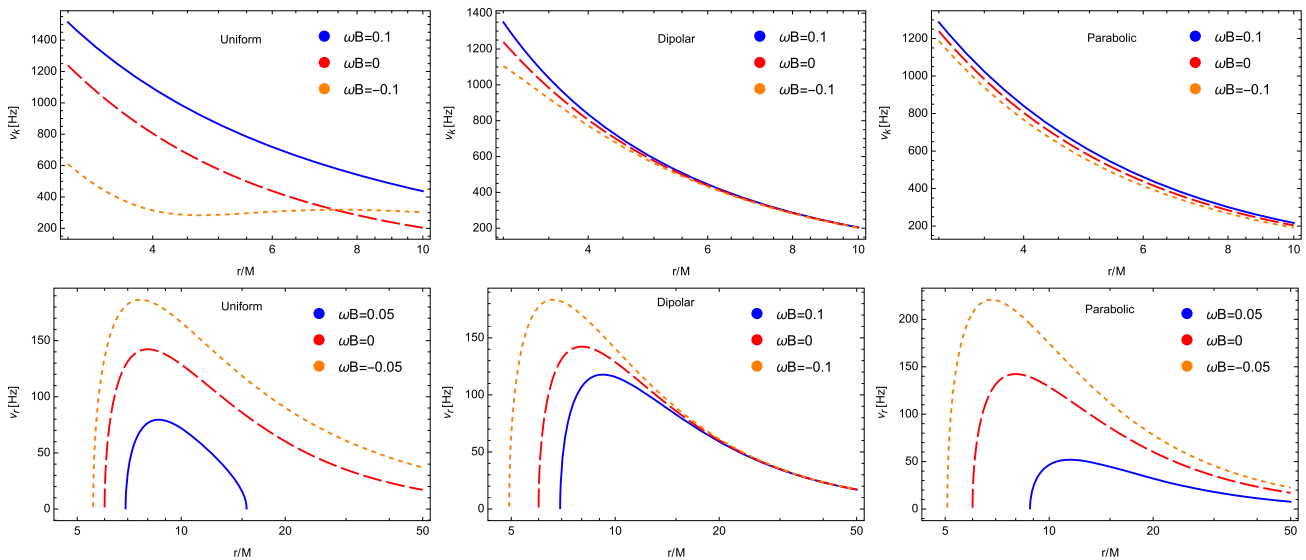


**Fig. 2** Keplerian (top row) and radial (bottom row) oscillation frequency against radial distance in dipolar (middle row), uniform (left column), and parabolic (right column) magnetic field

the effect of gravity becomes weaker and the motion of the particle just depends on the magnetic field. Both dipolar and parabolic fields decrease when  $r/M \rightarrow \infty$ , but the uniform field stays constant. Meanwhile, for the radial frequency, both the uniform and parabolic fields have a huge influence with a small  $\omega_B$ , while the dipolar field does not distort the graphs too much.

It is also observed from the bottom-left panel, which is a uniform case, that the frequency of radial oscillations at  $\omega_B = 0.05$  decrease and becomes zero about 15–18M. It means that there is a region of stable circular orbits between innermost and outermost ones for  $\omega > 0$ . Also, the wideness of the region decrease as  $\omega_B$  increase.

#### 4 Quasiperiodic oscillations in relativistic precession model

We study QPOs originated by charged particle oscillations orbiting the central Schwarzschild black hole embedded in external magnetic fields. We investigate relationships between upper and lower frequencies of twin peak QPOs around the magnetized Schwarzschild black hole, and we compare the obtained results on the frequency relation with the neutral particles orbiting both Schwarzschild and Kerr black holes [15].

First, we obtain equations for the upper and lower frequencies in the relativistic precession (RP) model where the upper and lower frequencies of twin peak QPOs are defined by the radial and orbital frequencies as  $\nu_U = \nu_\phi$  and  $\nu_L = \nu_\phi - \nu_r$ , respectively [49]. We provide graphical

analyses of the upper-lower frequency diagram in the dipolar, uniform, and parabolic magnetic field configuration cases.

Figure 3 demonstrates upper and lower frequencies for the external uniform, dipolar, and parabolic magnetic field configurations, as well as in the Schwarzschild and Kerr black hole cases without any external magnetic fields. Similar to Fig. 2, the uniform magnetic field model is the most sensitive to the value of  $\omega_B$ . On the other hand, by tuning the spin parameter  $a$  in the Kerr black hole, its curve can be made nearly overlapping any curve with finite  $\omega_B$  for dipolar and parabolic external magnetic fields. This means that both a Kerr black hole without an external magnetic field and a Schwarzschild black hole with a magnetic field can produce almost identical QPO frequencies by charged particles around them, and distinguishing the two cases requires other types of observational data and theoretical analysis. So, there is a degeneracy between the spin of the Kerr black holes and the external magnetic field around Schwarzschild black holes.

#### 5 Constraints on the BH mass and magnetic field

Testing gravity theories and astrophysical magnetic fields through data from observations is an important and actual issue in relativistic astrophysics. There are several observational data to obtain valuable information about gravitational properties of the spacetime and electromagnetic fields around astrophysical black holes. One of them is frequency data from QPOs observed in microquasars a binary system of a central compact object and companion star, in which the central massive object is assumed to be a candidate for (stellar-mass)

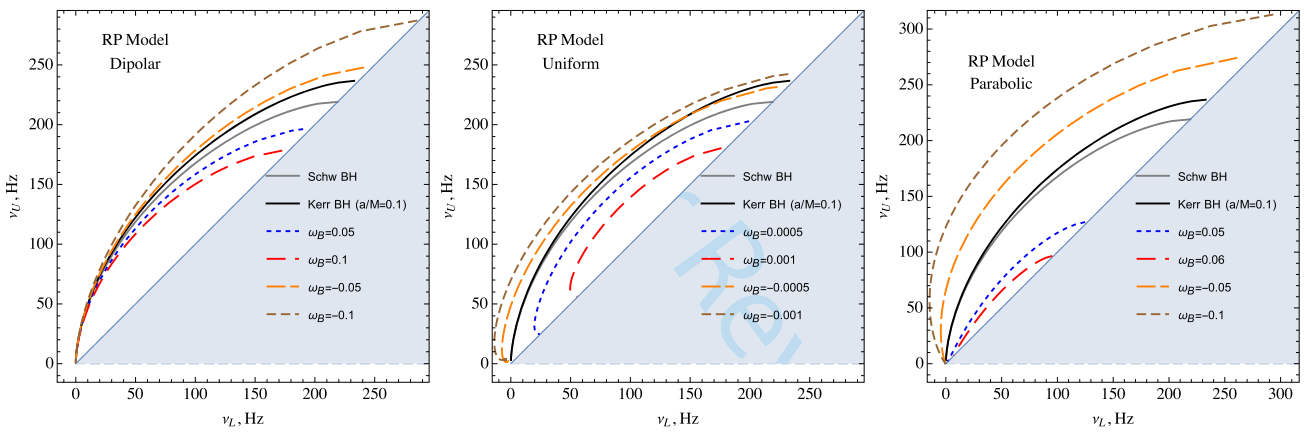


**Fig. 3** Upper versus lower QPO frequencies using RP model for dipolar (left), uniform (middle), and parabolic (right) magnetic field configurations

black holes. However, in realistic cases, it is impossible to know the exact type of black holes and magnetic field configurations. Therefore, we can test the black hole solutions and magnetic field configurations in theoretical studies of the origin mechanisms of QPOs.

In this section, we focus to get constraints on the magnetic field value around the Schwarzschild black hole and its mass using frequencies of the QPOs from the microquasars GRO J1655-40 and GRS 1915+105 assuming that the accreting matter surrounding the central black hole consists of charged particles primarily electrons and protons and the black hole is immersed in external magnetic fields with the uniform, dipolar and parabolic-like configurations. According to the relativistic precession model, the frequencies of the periastron precession  $\nu_{per}$  and the nodal precession  $\nu_{nod}$  are defined by the following relations:  $\nu_{per} = \nu_{\phi} - \nu_r$  and  $\nu_{nod} = \nu_{\phi} - \nu_{\theta}$ , respectively [49, 50].

In order to obtain the estimation for the five parameters as the peak frequencies of QPOs observed in the microquasars, we perform the  $\chi^2$  analysis with [51]

$$\chi^2(M, B, r_1, r_2) = \frac{(\nu_{1\phi} - \nu_{1U})^2}{\sigma_{1U}^2} + \frac{(\nu_{1per} - \nu_{1L})^2}{\sigma_{1L}^2} + \frac{(\nu_{1nod} - \nu_{1C})^2}{\sigma_{1C}^2} + \frac{(\nu_{2\phi} - \nu_{2U})^2}{\sigma_{2U}^2} + \frac{(\nu_{2nod} - \nu_{2C})^2}{\sigma_{2C}^2}. \tag{30}$$

In fact, the best estimates for the values of the parameters  $M$ ,  $\omega_B$ ,  $r_1$  and  $r_2$  should be at the minimum of  $\chi^2_{min}$  and the range of the parameters at the confidence level (C.L.) can be determined in the interval  $\chi^2_{min} + \Delta\chi^2$ .

### 5.1 GRO J1655-40

Here, we get constraints on the mass of the black hole and surrounding magnetic fields in the microquasar GRO J1655-40 using the two sets of QPO frequencies in the astrophysical observations [31],

$$\begin{aligned} \nu_{1U} &= 441 \text{ Hz}, \quad \sigma_{1U} = 2 \text{ Hz}, \\ \nu_{1L} &= 298 \text{ Hz}, \quad \sigma_{1L} = 4 \text{ Hz}, \\ \nu_{1C} &= 17.3 \text{ Hz}, \quad \sigma_{1C} = 0.1 \text{ Hz} \end{aligned} \tag{31}$$

and

$$\begin{aligned} \nu_{2U} &= 451 \text{ Hz}, \quad \sigma_{2U} = 5 \text{ Hz}, \\ \nu_{2C} &= 18.3 \text{ Hz}, \quad \sigma_{2C} = 0.1 \text{ Hz}. \end{aligned} \tag{32}$$

### 5.2 GRS 1915+105

Also, we perform a similar analysis on the GRS 1915 + 105 microquasar with QPO frequencies [52],

$$\begin{aligned} \nu_{1U} &= 184.10 \text{ Hz}, \quad \sigma_{1U} = 1.84 \text{ Hz}, \\ \nu_{2U} &= 142.98 \text{ Hz}, \quad \sigma_{2U} = 3.48 \text{ Hz}, \end{aligned} \tag{33}$$

and

$$\begin{aligned} \nu_{1L} &= 67.40 \text{ Hz}, \quad \sigma_{1L} = 0.60 \text{ Hz}, \\ \nu_{2L} &= 65.89 \text{ Hz}, \quad \sigma_{2L} = 0.52 \text{ Hz}, \\ \nu_{3L} &= 69.58 \text{ Hz}, \quad \sigma_{3L} = 0.49 \text{ Hz}. \end{aligned} \tag{34}$$

In Fig. 4 we have provided the best values of  $\omega_B$  and mass of the central black hole at the center of GRO J1655-40 immersed in an external uniform (left panel) and dipolar (right panel) magnetic fields. Furthermore, we present the contour levels  $1\sigma$ ,  $2\sigma$ , and  $3\sigma$  of  $\omega_B$  and  $M/M_{\odot}$ . The best-fit values of the radii of the circular orbits associated with the two sets of QPOs in GRO J1655-40 (GRS 1915+105) are found to be about  $r_1 = 3.46M$ ,  $r_2 = 5.15M$  ( $r_1 = 5.14M$ ,

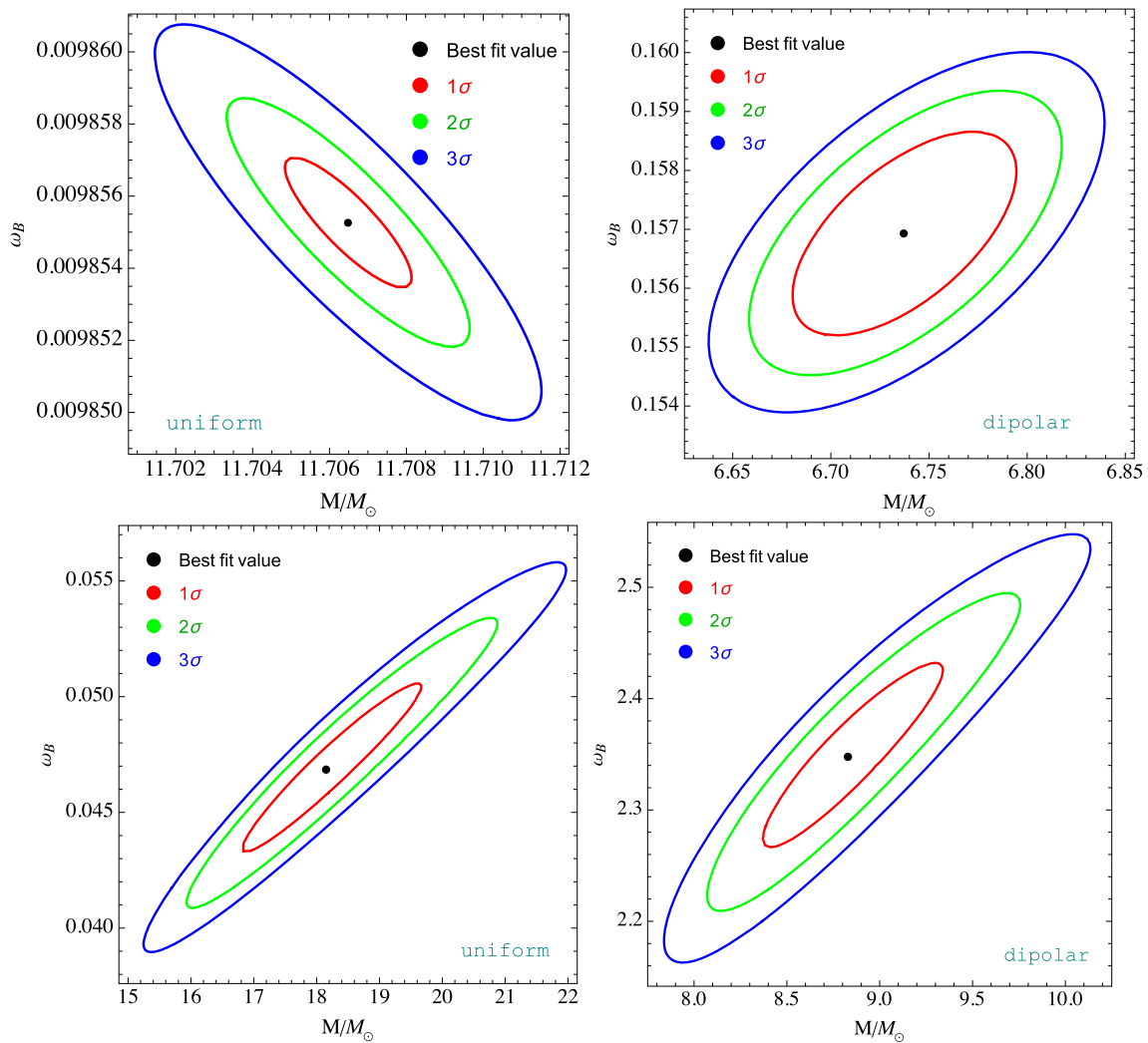


**Fig. 4** Constraints on the black hole mass and the magnetic field parameter for GRO J1655-40 (top row) and GRS 1915+105 (bottom row) in uniform (left panel) and dipolar (right panel) magnetic field configurations

$r_2 = 7.97M$ ) and  $r_1 = 4.67M$ ,  $r_2 = 4.77M$  ( $r_1 = 4.74M$ ,  $r_2 = 7.69M$ ) for uniform and dipolar magnetic fields, respectively. Also, it is obtained that the magnetic coupling parameter is about 0.0098 & 0.157 (0.047 & 2.35) and the black hole mass is about 11.7 & 6.737 (18.2 & 8.83) solar mass in uniform and dipolar magnetic field models for the microquasar GRO J1655-40 (GRS 1915+105).

### 5.3 Estimating magnetic field values

In this subsection, we get constraints on magnetic field strength by treating electrons and protons as test-charged particles. In the accretion disk of black holes, the astrophysical plasma consists of ions and electrons because of the high temperature in the accretion disc. Since hydrogen is likely the most abundant ion in the disk, we choose electrons and protons as concrete examples.

In plasma, collective behavior in the motion of charged particles arises due to the interplay between induced electric and magnetic fields and the motion of charged particles. Collective motion gives rise to phenomena such as plasma waves, instabilities, and other collective modes in particle oscillations. So, the dynamics of the system are better described by the MHD equations rather by those of single particle motion. Although this would prevent a particle or a charged fluid element from experiencing the exact same dynamics as described in Sect. 3, we have decided to neglect plasma effects to show a potential application of the results presented above. It is out of the scope of this paper to study to what extent this is a suitable approximation for the system under study

Figure 5 presents the estimates of black hole mass  $M$  and magnetic field  $B$  using a uniform magnetic field (top row) and dipolar magnetic field (bottom row) configurations. It is

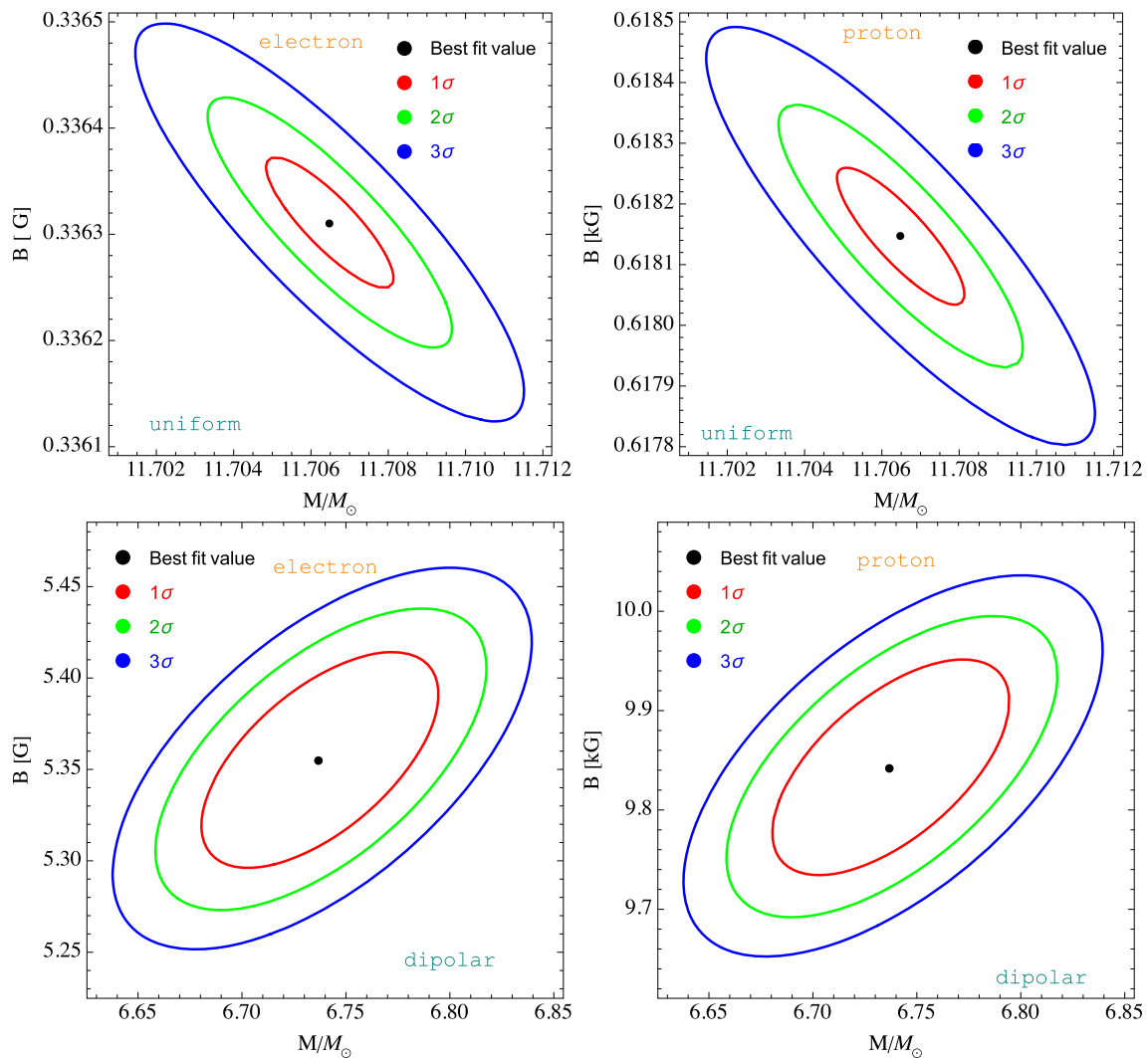


**Fig. 5** Constraints on the black hole mass and magnetic field values for GRO J1655-40 in uniform (top row) and dipolar (bottom row) magnetic field configurations for the electron (left column) proton (right column)

found that the parabolic magnetic field model disagrees with the observed data, so constraints are not presented. Therefore, we can obtain constraints on the black hole mass and magnetic field for the dipolar and uniform magnetic field configuration cases. Since there are five degrees of freedom in the observational data, we have taken the values for  $\Delta\chi^2$ , 5.89, 11.29, and 17.96 corresponding to the error bar  $1\sigma$ ,  $2\sigma$ , and  $3\sigma$ , which gives confidence level 68.3%, 95.4%, and 99.7%, respectively. The dipolar field model gives the best-fit values of mass  $M/M_{\odot} = 6.737^{+0.061}_{-0.055}$  and magnetic field value  $B[G] = 5.355^{+0.058}_{-0.061}$  for the case where the charged particle tested is an electron, and for the uniform field model, the black hole mass is  $M/M_{\odot} = 11.707 \pm 0.002$ , and the magnetic field value  $B[G] = 0.3363^{+0.0007}_{-0.0005}$ . If the charged particle is a proton, then the dipolar field is  $B[kG] = 9.85^{+0.12}_{-0.13}$  and the uniform field is  $B[kG] = 0.618 \pm 0.001$ .

Figure 6 presents the estimates of the central black hole mass  $M$  and the magnetic field  $B$  around it for the uniform magnetic field (top row) and dipolar magnetic field (bottom row) configurations using the same confidence levels as in Sect. 5.1. The dipolar field model gives  $M/M_{\odot} = 8.83^{+0.53}_{-0.48}$ , and  $B[G] = 80.12^{+2.38}_{-2.86}$  for electrons. The uniform field model gives  $M/M_{\odot} = 18.2^{+1.6}_{-1.4}$ , and  $B[G] = 1.60 \pm 0.13$  for electron. Moreover, in the case when the charged particle is a proton, the dipolar field  $B[kG] = 147.4^{+4.4}_{-5.3}$  and uniform field  $B[kG] = 2.94 \pm 0.24$  with the same mass as obtained in the electron case.

#### 5.4 Comparisons of black hole mass constraints

The independent observations of the X-ray timing techniques estimated that the central black hole in the microquasar GRO J1655-40 has mass  $M/M_{\odot} = 5.31 \pm 0.07$  [53]. While esti-

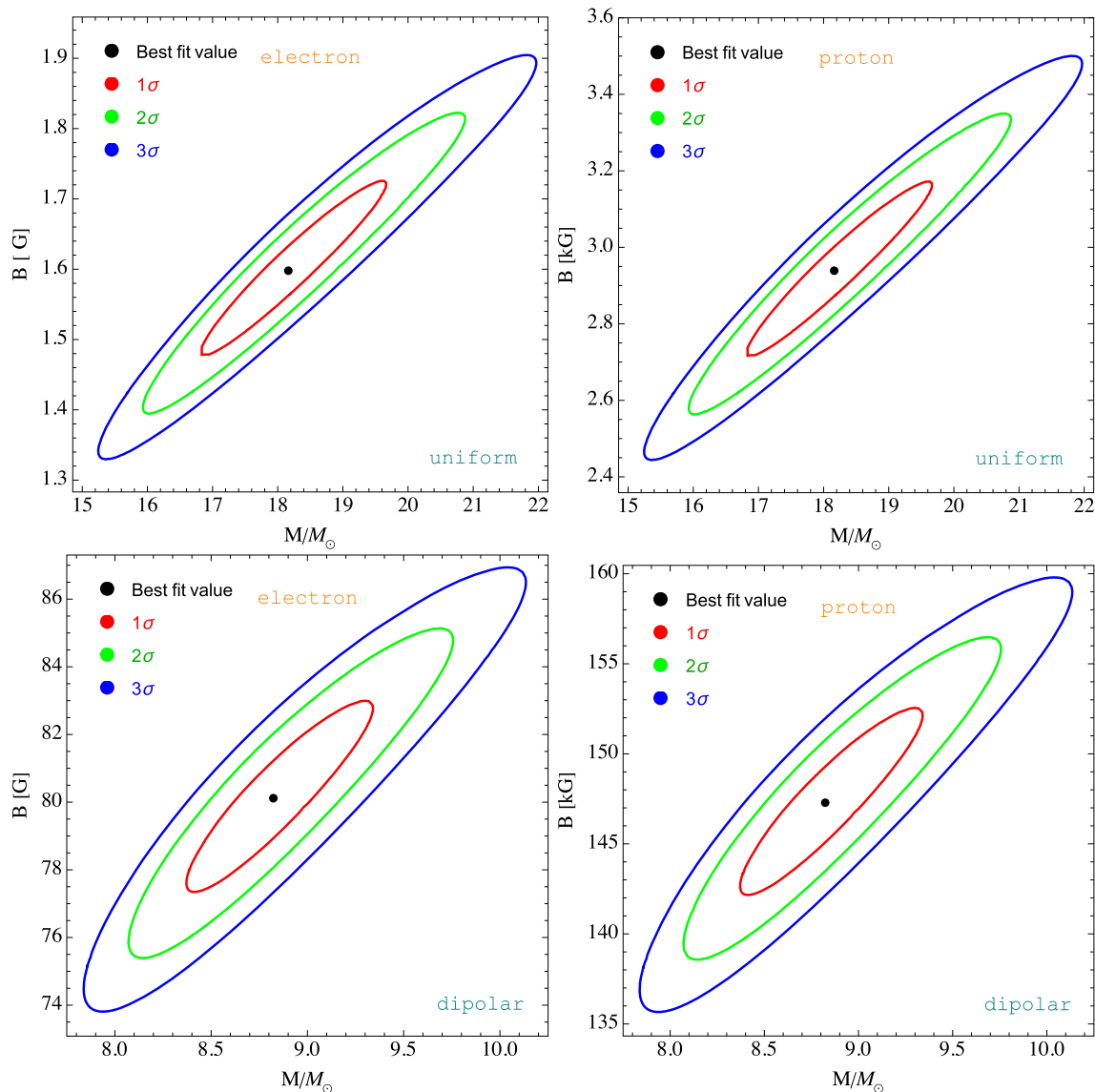


**Fig. 6** The same figure with Fig. 5, but for the microquasar GRS 1915+105

mations on the black hole mass using QPOs around rotating Kerr black holes generated by charged test particles without external magnetic field in the RP model have shown that is about  $M/M_{\odot} = 5.3 \pm 0.1$  [54]. The constraints are close to that value what we have got in the dipolar magnetic field case ( $\sim 6.7M_{\odot}$ ). However, both mass constrains are significantly smaller than our findings in uniform magnetic case. This implies that the magnetic field near the microquasar where the accretion disk is located is better suited for dipolar magnetic field configuration.

The infrared spectroscopy technique estimates that the central black hole in the microquasar GRS 1915+105 has mass  $M/M_{\odot} = 12 \pm 1.4$  [55]. Authors in Ref. [56] have studied QPOs around rotating Kerr black holes in the absence of magnetic field in the RP model, and have estimated that the

mass of the central black hole is about  $M/M_{\odot} = 13.1 \pm 0.2$ . In this case, our constraints on the black hole mass in both dipolar and uniform magnetic field configurations are sufficiently different from the above ones, with the dipolar field configuration results being slightly closer. This suggests the magnetic field in the microquasar GRS 1915+105 may be dipole-like, but the results are not fully conclusive.

## 6 Discussions and conclusions

The idea of this paper is to explore the possibility of getting constraints on the black hole mass and magnetic field values around of the central black hole in the microquasars using observed QPO frequencies.

In the present work, we have assumed Schwarzschild black holes are immersed in external magnetic fields with asymptotically uniform, dipolar, and parabolic configurations. Then, we studied the dynamics of charged test particles around the magnetized Schwarzschild black hole. We also calculated the oscillation frequencies of the charged particles along stable circular orbits in the vertical and radial directions.

It is obtained that the Keplerian frequency of the particles in the parabolic magnetic field is smaller than the uniform and dipolar ones. However, the frequencies of radial oscillations are bigger in the parabolic case with compare to the other configurations. It is also found that in the presence of a uniform magnetic field with positive  $\omega_B$  there are two limits for stable circular orbits: inner (ISCO) and outer (OSCO) where radial oscillation frequency is zero. The distance between ISCO and OSCO is called the width of the accretion disc consisting of charged particles. Also, this width is negatively correlated to the value of  $\omega_B$ .

We have also investigated the effect of the external magnetic fields on the upper and lower frequencies of twin-peak QPOs in the RP model. Our analyses have shown that the frequency ratio increases (decreases) for  $\omega_B < 0$  ( $\omega_B > 0$ ) for the three magnetic field configurations. Furthermore, the ratio is more sensitive to the field strength in the uniform case than in dipole and parabolic cases.

We have obtained constraints on the central black hole mass and the magnetic field parameter by applying  $\chi^2$  analysis by fitting observational data from observed frequencies of QPOs in microquasars GRO J1655-40 and GRS 1915+105 in the RP model. Our numerical results have shown that the uniform and dipolar field models can fit the observation data and could be a source of QPOs, however, the parabolic magnetic field can not fit the observational QPO data. Also, it is obtained that the magnetic coupling parameter is about 0.0098 & 0.157 (0.047 & 2.35) and the black hole mass is about 11.7 & 6.737 (18.2 & 8.83) solar mass in uniform and dipolar magnetic field models for the microquasar GRO J1655-40 (GRS 1915+105).

Finally, to obtain estimations for magnetic field values, we have treated electrons and protons as test-charged particles. Our  $\chi^2$  analyses have shown that for the dipolar magnetic field configuration when the test charged particles are treated as electrons, the best-fit values of the central black hole mass  $M/M_\odot = 6.737^{+0.061}_{-0.055}$  in the microquasar GRO J1655-40, and the magnetic field around the central black hole is  $B[G] = 5.355^{+0.058}_{-0.061}$ , and for the uniform field configuration, the black hole mass is  $M/M_\odot = 11.707 \pm 0.002$ , and the magnetic field value is  $B[G] = 0.3363^{+0.0007}_{-0.0005}$ .

The results for the microquasars GRS 1915+105 have shown that the dipolar field model gives  $M/M_\odot = 8.83^{+0.53}_{-0.48}$ , and  $B[G] = 80.12^{+2.38}_{-2.86}$  for electrons. The uniform field

model gives  $M/M_\odot = 18.2^{+1.6}_{-1.4}$ , and  $B[G] = 1.60 \pm 0.13$  for protons.

**Acknowledgements** This research is also supported by Grants No. F-FA-2021-432 and No. F-FA-2021-510 of the Uzbekistan Agency for Innovative Development. B.A. and J.R. acknowledge the ERASMUS+ ICM project for supporting their stay at the Silesian University in Opava.

**Data Availability Statement** This manuscript has no associated data or the data will not be deposited. [Authors' comment: Our paper has pure theoretical behavior.]

**Open Access** This article is licensed under a Creative Commons Attribution 4.0 International License, which permits use, sharing, adaptation, distribution and reproduction in any medium or format, as long as you give appropriate credit to the original author(s) and the source, provide a link to the Creative Commons licence, and indicate if changes were made. The images or other third party material in this article are included in the article's Creative Commons licence, unless indicated otherwise in a credit line to the material. If material is not included in the article's Creative Commons licence and your intended use is not permitted by statutory regulation or exceeds the permitted use, you will need to obtain permission directly from the copyright holder. To view a copy of this licence, visit <http://creativecommons.org/licenses/by/4.0/>.

Funded by SCOAP<sup>3</sup>. SCOAP<sup>3</sup> supports the goals of the International Year of Basic Sciences for Sustainable Development.

## References

1. A. Ingram, M. van der Klis, M. Middleton, C. Done, D. Altamirano, L. Heil, P. Uttley, M. Axelsson, *Mon. Not. R. Astron. Soc.* **461**(2), 1967 (2016). <https://doi.org/10.1093/mnras/stw1245>
2. C. Bambi, *Black Holes: A Laboratory for Testing Strong Gravity* (Springer, Singapore, 2017)
3. Z. Stuchlík, M. Kološ, *Mon. Not. R. Astron. Soc.* **451**(3), 2575 (2015). <https://doi.org/10.1093/mnras/stv1120>
4. G. Török, K. Goluchová, E. Šrámková, M. Urbanec, O. Straub, *Mon. Not. R. Astron. Soc.* **488**(3), 3896 (2019). <https://doi.org/10.1093/mnras/stz1929>
5. Z. Stuchlík, A. Kotrlová, G. Török, *Astron. Astrophys.* **525**, A82 (2011). <https://doi.org/10.1051/0004-6361/201015029>
6. G. Török, A. Kotrlová, E. Šrámková, Z. Stuchlík, *Astron. Astrophys.* **531**, A59 (2011). <https://doi.org/10.1051/0004-6361/201015549>
7. J. Rayimbaev, P. Tadjimuratov, A. Abdujabbarov, B. Ahmedov, M. Khudoyberdieva, *Galaxies* **9**(4), 75 (2021). <https://doi.org/10.3390/galaxies9040075>
8. J. Rayimbaev, B. Ahmedov, A.H. Bokhari, *Int. J. Mod. Phys. D* **31**(11), 2240004–726 (2022). <https://doi.org/10.1142/S0218271822400041>
9. J. Rayimbaev, A. Abdujabbarov, F. Abdulkhamidov, V. Khamidov, S. Djumanov, J. Toshov, S. Inoyatov, *Eur. Phys. J. C* **82**(12), 1110 (2022). <https://doi.org/10.1140/epjc/s10052-022-11080-8>
10. J. Rayimbaev, P. Tadjimuratov, A. Abdujabbarov, B. Ahmedov, M. Khudoyberdieva, *Galaxies* **9**(4), 75 (2021). <https://doi.org/10.3390/galaxies9040075>
11. J. Rayimbaev, A.H. Bokhari, B. Ahmedov, *Class. Quantum Gravity* **39**(7), 075021 (2022). <https://doi.org/10.1088/1361-6382/ac556a>
12. L. Angelini, L. Stella, A.N. Parmar, *Astrophys. J.* **346**, 906 (1989). <https://doi.org/10.1086/168070>
13. G. Török, M.A. Abramowicz, Z. Stuchlík, E. Šrámková, in *Binary Stars as Critical Tools & Tests in Contemporary Astrophysics*, vol.

- 240, ed. by W.I. Hartkopf, P. Harmanec, E.F. Guinan, vol. 240, pp. 724–726 (2007). <https://doi.org/10.1017/S1743921307006473>
14. G. Török, Z. Stuchlík, *Astron. Astrophys.* **437**(3), 775 (2005). <https://doi.org/10.1051/0004-6361:20052825>
15. Z. Stuchlík, M. Kološ, *Astron. Astrophys.* **586**, A130 (2016). <https://doi.org/10.1051/0004-6361/201526095>
16. L. Rezzolla, S. Yoshida, T.J. Maccarone, O. Zanotti, *Mon. Not. R. Astron. Soc.* **344**, L37 (2003). <https://doi.org/10.1046/j.1365-8711.2003.07018.x>
17. L. Rezzolla, O. Zanotti, J.A. Pons, *J. Fluid Mech.* **479**, 199 (2003)
18. L. Rezzolla, S. Yoshida, O. Zanotti, *Mon. Not. R. Astron. Soc.* **344**, 978 (2003). <https://doi.org/10.1046/j.1365-8711.2003.07023.x>
19. J. Rayimbaev, A. Abdujabbarov, H. Wen-Biao, *Phys. Rev. D* **103**(10), 104070 (2021). <https://doi.org/10.1103/PhysRevD.103.104070>
20. J. Rayimbaev, A. Abdujabbarov, M. Jamil, B. Ahmedov, W.B. Han, *Phys. Rev. D* **102**, 084016 (2020). <https://doi.org/10.1103/PhysRevD.102.084016>
21. I.D. Novikov, K.S. Thorne, in *Black Holes (Les Astres Occlus)*, ed. by C. Dewitt, B.S. Dewitt (1973), pp. 343–450
22. N.I. Shakura, R.A. Sunyaev, *Astron. Astrophys.* **24**, 337 (1973)
23. M.A. Abramowicz, A. Lanza, E.A. Spiegel, E. Szuszkiewicz, *Nature* **356**(6364), 41 (1992). <https://doi.org/10.1038/356041a0>
24. L. Stella, M. Vietri, *Astrophys. J. Lett.* **492**(1), L59 (1998). <https://doi.org/10.1086/311075>
25. A. Čadež, M. Calvani, U. Kostić, *Astron. Astrophys.* **487**(2), 527 (2008). <https://doi.org/10.1051/0004-6361:200809483>
26. U. Kostić, A. Čadež, M. Calvani, A. Gomboc, *Astrophys. Astron.* **496**(2), 307 (2009). <https://doi.org/10.1051/0004-6361/200811059>
27. M.A. Abramowicz, W. Kluźniak, *Astron. Astrophys.* **374**, L19 (2001). <https://doi.org/10.1051/0004-6361:20010791>
28. P. Bakala, G. Török, V. Karas, M. Dovčiak, M. Wildner, D. Wzientek, E. Šrámková, M. Abramowicz, K. Goluchová, G.P. Mazur, F.H. Vincent, *Mon. Not. R. Astron. Soc.* **439**(2), 1933 (2014). <https://doi.org/10.1093/mnras/stu076>
29. G.D. Karssen, M. Bursa, A. Eckart, M. Valencia-S, M. Dovčiak, V. Karas, J. Horák, *Mon. Not. R. Astron. Soc.* **472**(4), 4422 (2017). <https://doi.org/10.1093/mnras/stx2312>
30. C. Germanà, *Phys. Rev. D* **96**(10), 103015 (2017). <https://doi.org/10.1103/PhysRevD.96.103015>
31. Z. Stuchlík, A. Kotrlová, G. Török, *Astron. Astrophys.* **552**, A10 (2013). <https://doi.org/10.1051/0004-6361/201219724>
32. S. Kato, *J. Fukue, Publ. Astron. Soc. Jpn.* **32**, 377 (1980)
33. A.T. Okazaki, S. Kato, *J. Fukue, Publ. Astron. Soc. Jpn.* **39**, 457 (1987)
34. M.A. Nowak, R.V. Wagoner, *Astrophys. J.* **393**, 697 (1992). <https://doi.org/10.1086/171538>
35. R.V. Wagoner, *Phys. Rep.* **311**, 259 (1999). [https://doi.org/10.1016/S0370-1573\(98\)00104-5](https://doi.org/10.1016/S0370-1573(98)00104-5)
36. R.V. Wagoner, A.S. Silbergleit, M. Ortega-Rodríguez, *Astrophys. J. Lett* **559**(1), L25 (2001). <https://doi.org/10.1086/323655>
37. A.S. Silbergleit, R.V. Wagoner, M. Ortega-Rodríguez, *Astrophys. J.* **548**(1), 335 (2001). <https://doi.org/10.1086/318659>
38. D.H. Wang, L. Chen, C.M. Zhang, Y.J. Lei, J.L. Qu, L.M. Song, *Mon. Not. R. Astron. Soc.* **454**(2), 1231 (2015). <https://doi.org/10.1093/mnras/stv1999>
39. L. Rezzolla, S. Yoshida, T.J. Maccarone, O. Zanotti, *Mon. Not. R. Astron. Soc.* **344**(3), L37 (2003). <https://doi.org/10.1046/j.1365-8711.2003.07018.x>
40. A. Ingram, C. Done, *Mon. Not. R. Astron. Soc.* **405**(4), 2447 (2010). <https://doi.org/10.1111/j.1365-2966.2010.16614.x>
41. P.C. Fragile, O. Straub, O. Blaes, *Mon. Not. R. Astron. Soc.* **461**(2), 1356 (2016). <https://doi.org/10.1093/mnras/stw1428>
42. Z. Stuchlík, A. Kotrlová, G. Török, *Acta Astron.* **62**(4), 389 (2012)
43. M. Ortega-Rodríguez, H. Solís-Sánchez, L. Álvarez-García, E. Doderó-Rojas, *Mon. Not. R. Astron. Soc.* **492**(2), 1755 (2020). <https://doi.org/10.1093/mnras/stz3541>
44. A. Maselli, G. Pappas, P. Pani, L. Gualtieri, S. Motta, V. Ferrari, L. Stella, *Astrophys. J.* **899**(2), 139 (2020). <https://doi.org/10.3847/1538-4357/ab9ff4>
45. R.M. Wald, *Phys. Rev. D* **10**, 1680 (1974). <https://doi.org/10.1103/PhysRevD.10.1680>
46. J.A. Petterson, *Phys. Rev. D* **10**, 3166 (1974). <https://doi.org/10.1103/PhysRevD.10.3166>
47. M. Nakamura, K. Asada, K. Hada, H.Y. Pu, S. Noble, C. Tseng, K. Toma, M. Kino, H. Nagai, K. Takahashi, J.C. Algaba, M. Orienti, K. Akiyama, A. Doi, G. Giovannini, M. Giroletti, M. Honma, S. Koyama, R. Lico, K. Niinuma, F. Tazaki, *Astrophys. J.* **868**(2), 146 (2018). <https://doi.org/10.3847/1538-4357/aaeb2d>
48. L. Rezzolla, B.J. Ahmedov, J.C. Miller, *Mon. Not. R. Astron. Soc.* **322**, 723 (2001). <https://doi.org/10.1046/j.1365-8711.2001.04161.x>
49. L. Stella, M. Vietri, S.M. Morsink, *Astrophys. J.* **524**(1), L63 (1999). <https://doi.org/10.1086/312291>
50. J. Rayimbaev, B. Majeed, M. Jamil, K. Jusufi, A. Wang, *Phys. Dark Univ.* **35**, 100930 (2022). <https://doi.org/10.1016/j.dark.2021.100930>
51. C. Bambi, (2013). [arXiv:1312.2228](https://arxiv.org/abs/1312.2228)
52. T. Belloni, P. Soleri, P. Casella, M. Méndez, S. Migliari, *Mon. Not. R. Astron. Soc.* **369**(1), 305 (2006). <https://doi.org/10.1111/j.1365-2966.2006.10286.x>
53. S.E. Motta, T.M. Belloni, L. Stella, T. Muñoz-Darias, R. Fender, *Mon. Not. R. Astron. Soc.* **437**(3), 2554 (2014). <https://doi.org/10.1093/mnras/stt2068>
54. Z. Stuchlík, M. Kološ, *Astrophys. J.* **825**(1), 13 (2016). <https://doi.org/10.3847/0004-637X/825/1/13>
55. D.J. Hurley, P.J. Callanan, P. Elebert, M.T. Reynolds, *Mon. Not. R. Astron. Soc.* **430**(3), 1832 (2013). <https://doi.org/10.1093/mnras/stt001>
56. S. Kato, *PASJ* **56**, L25 (2004). <https://doi.org/10.1093/pasj/56.5.L25>